small methods

Supporting Information

for *Small Methods,* DOI: 10.1002/smtd.202100508

Core–Shell MOF-in-MOF Nanopore Bifunctional Host of Electrolyte for High-Performance Solid-State Lithium Batteries

Ahmed Eissa Abdelmaoula, Jun Shu, Yu Cheng, Lin Xu, Gang Zhang, Yangyang Xia, Muhammad Tahir, Peijie Wu, and Liqiang Mai**

Supporting Information

Core-shell MOF-in-MOF nanopores bi-functional host of electrolyte for high-performance solid-state lithium batteries

Ahmed Eissa Abdelmaoula,[1,3] *Jun Shu,*[1] *Yu Cheng,*[1] *Lin Xu,*[1, 2,*] *Gang Zhang,*[1] *Yangyang Xia,*[1] *Muhammad Tahir,*[1] *Peijie Wu,*[1] *and Liqiang Mai* [1, 2,*]

[1] State Key Laboratory of Advanced Technology for Materials Synthesis and Processing, School of Materials Science and Engineering, Wuhan University of Technology, Wuhan 430070, China.

[2] Foshan Xianhu Laboratory of the Advanced Energy Science and Technology Guangdong Laboratory, Xianhu hydrogen Valley, Foshan 528200, China.

[3] Mining and Metallurgical Department, Faculty of Engineering, Al-Azhar University, Cairo, Egypt.

* Corresponding author: linxu@whut.edu.cn; mlq518@whut.edu.cn.

KEYWORDS: Core-shell, electrochemical energy storage, bi-functional host, lithium-ion batteries.

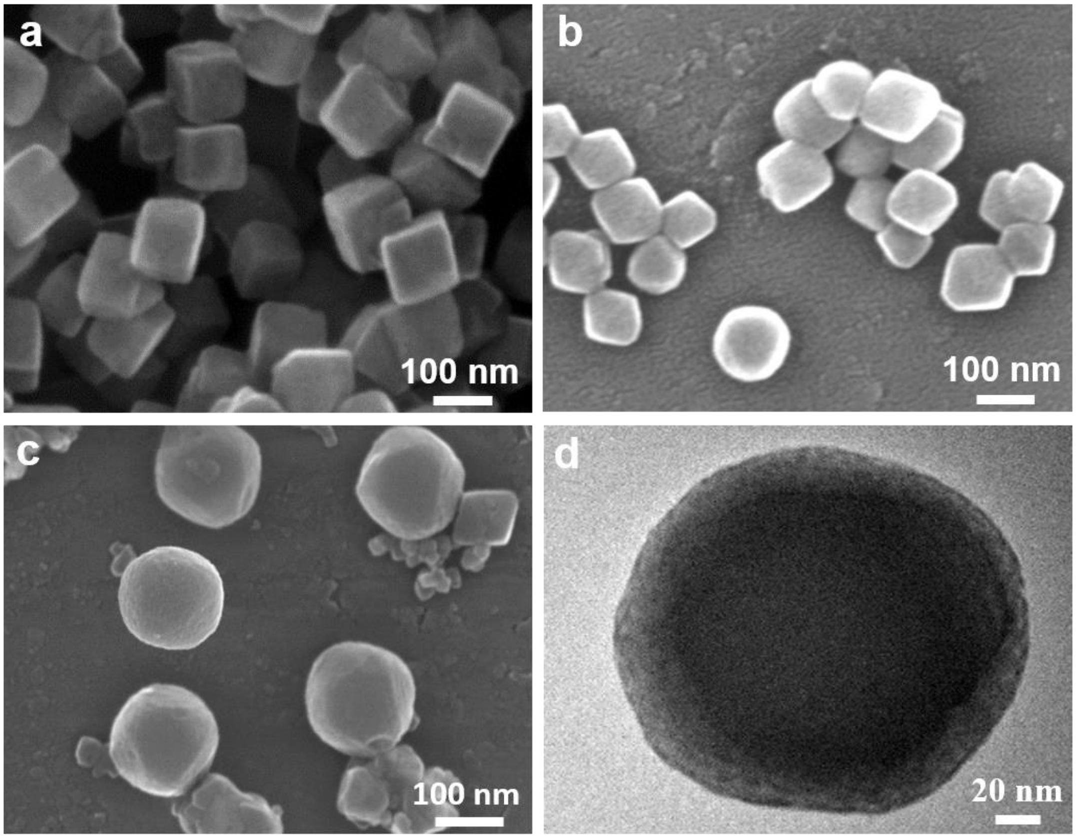

Figure S1. a, b, c) SEM images of UIO-66, UIO-67 and UIO-66@67 respectively. d) TEM image of UIO-66@67.

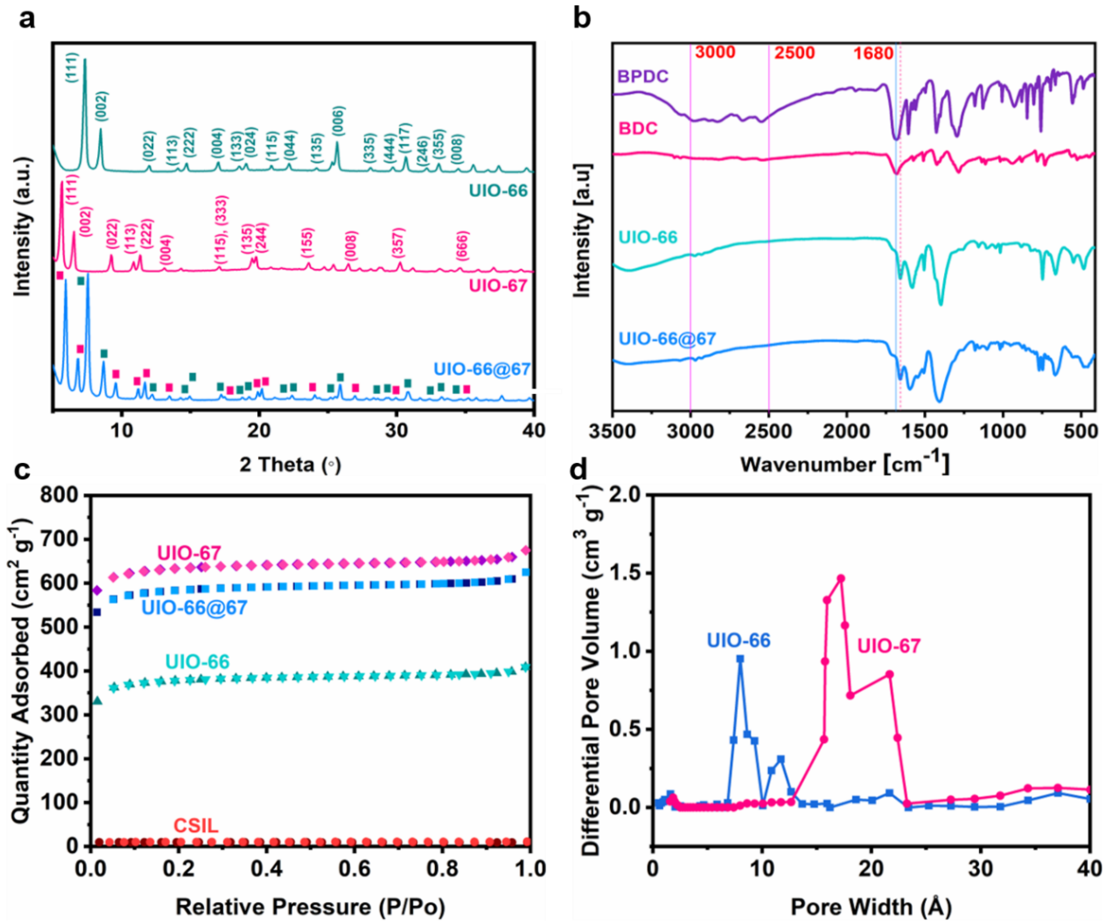

Figure S2. a) X-ray diffraction patterns of the as-prepared UIO-66, UIO-67 and UIO-66@67 The green dots indicate the peaks of UIO-66 and the red dots indicate the peaks of UIO-67. b) FT-IR characterization of BPDC, BDC, UIO-66 and UIO-66@67 c) N_2 adsorption/desorption isothermal linear plots of UIO-66, UIO-67, UIO-66@67 and CSIL. d) Statistical particle size distribution of UIO-66 and UIO-67.

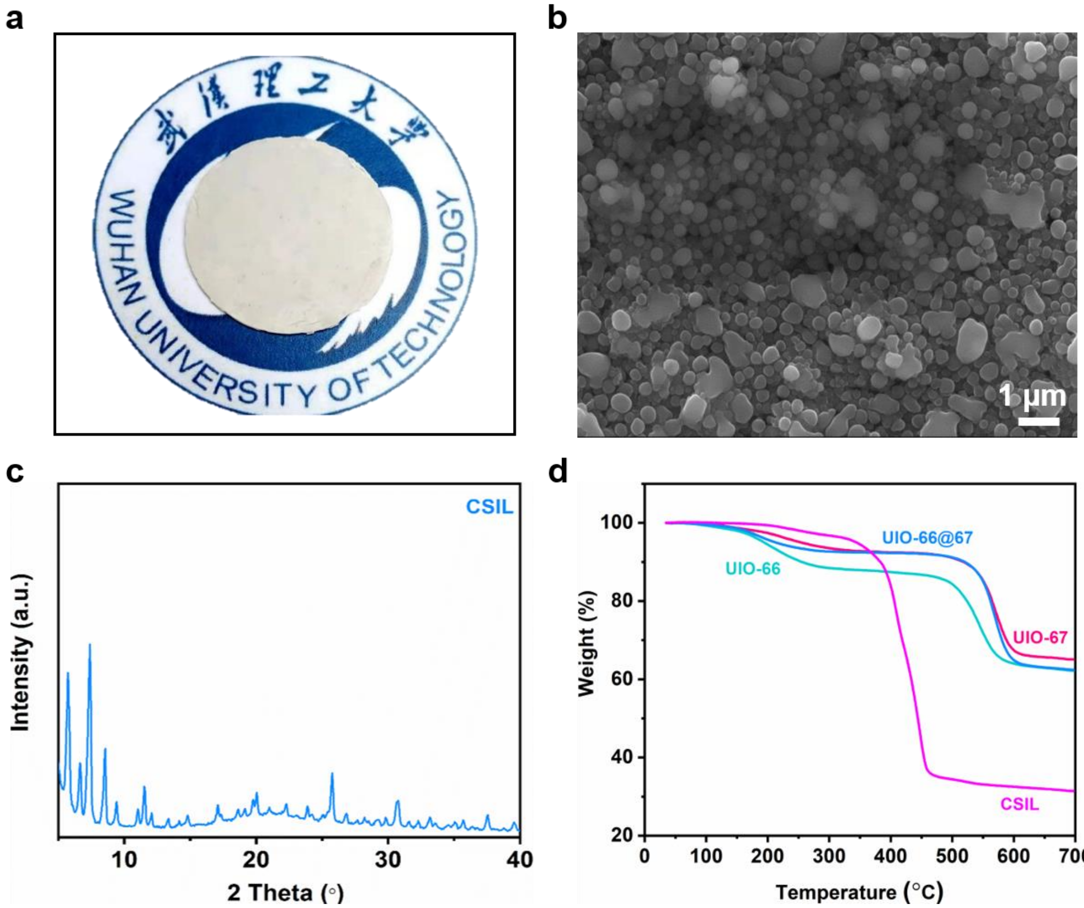

Figure S3. a) The photograph of CSIL solid electrolyte. b) SEM image of CSIL solid electrolyte. c) XRD patterns of compacting CSIL solid electrolyte at 30MPa. d) TGA curve of UIO-66, UIO-67, UIO-66@67 and CSIL.

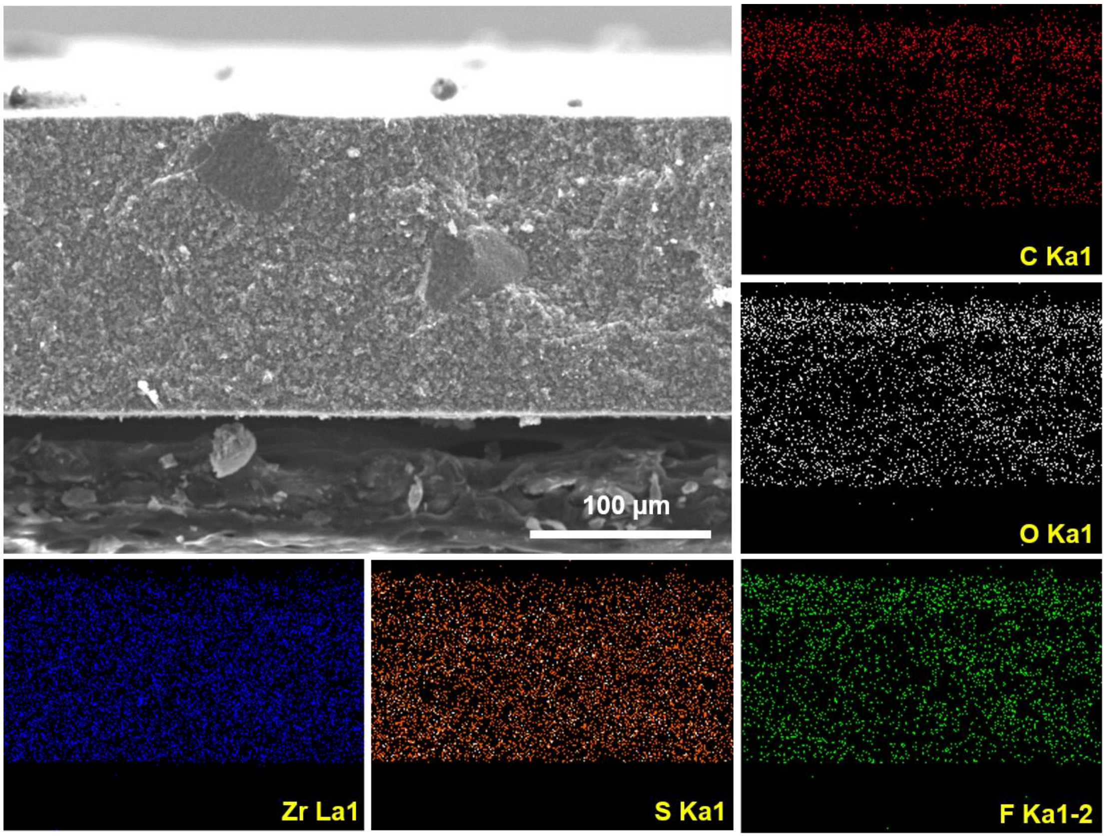

Figure S4. The cross-section of CSIL solid electrolyte with elemental mapping of C, O, Zr, S and F.

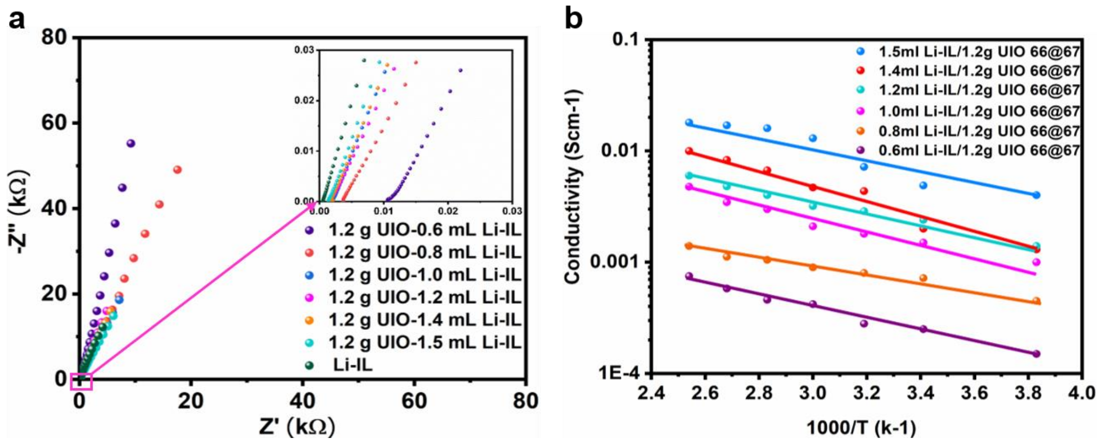

Figure S5. a) EIS of CSIL solid electrolyte with different composition and Li-IL at room temperature. b) Arrhenius plots of CSIL solid electrolyte with different composition and temperature.

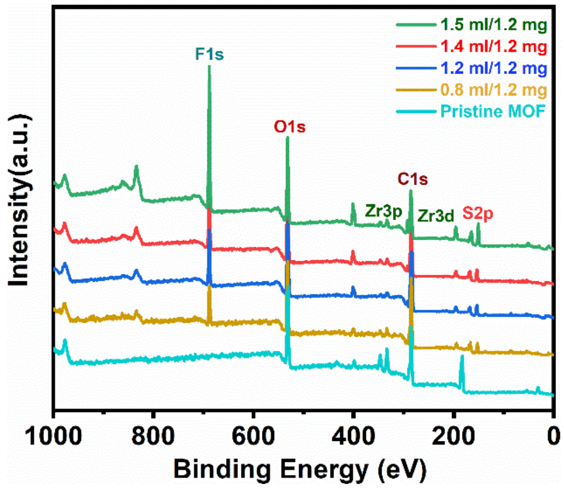

Figure S6. XPS spectra wide survey of CSLI filler metal with different Li-IL amount and pristine MOF.

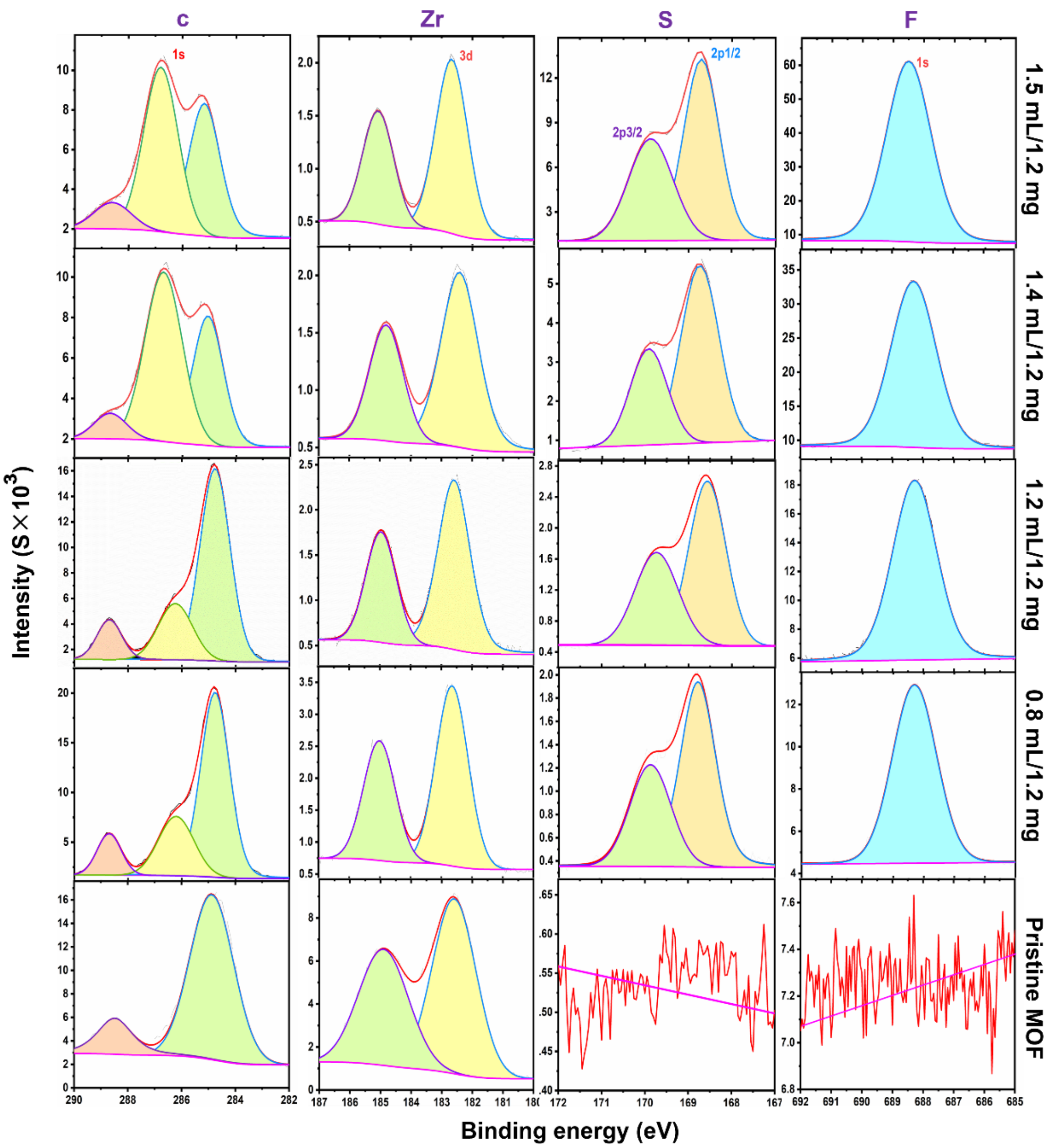

Figure S7. XPS spectra of CSIL with different amount of Li-IL and pristine MOF.

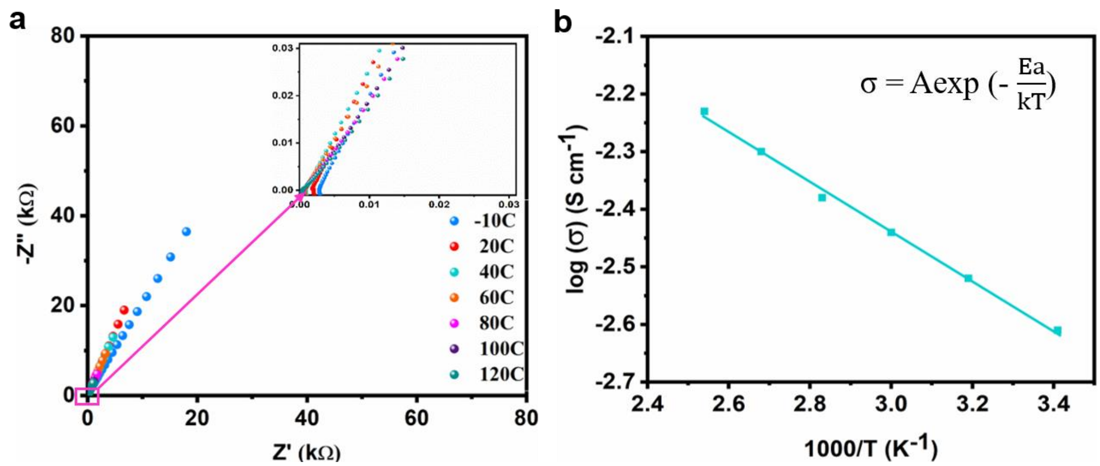

Figure S8. a) EIS of CSIL solid electrolyte with composition 1.2 mL:1.2 mg at different temperature, b) Arrhenius plots of CSIL solid electrolyte with 1.2 g UIO-66@67 to 1.2 ml Li-IL composition at deferent temperature.

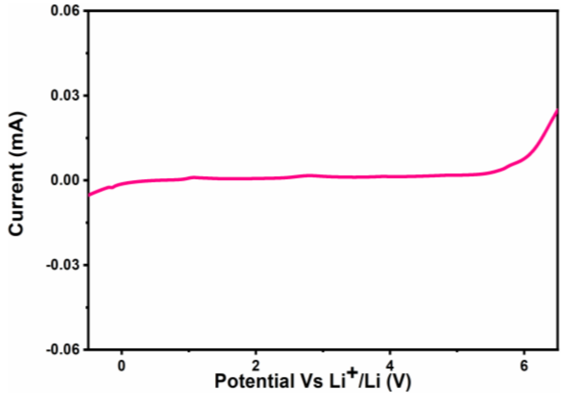

Figure S9. Linear sweep voltammogram of CSIL solid electrolyte at a scan rate of 0.5mV and 25 ˚C.

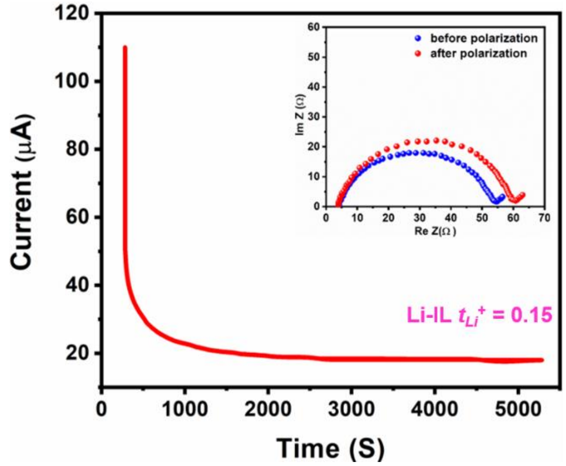

Figure S10. DC polarization curve of Li-IL at room temperature.

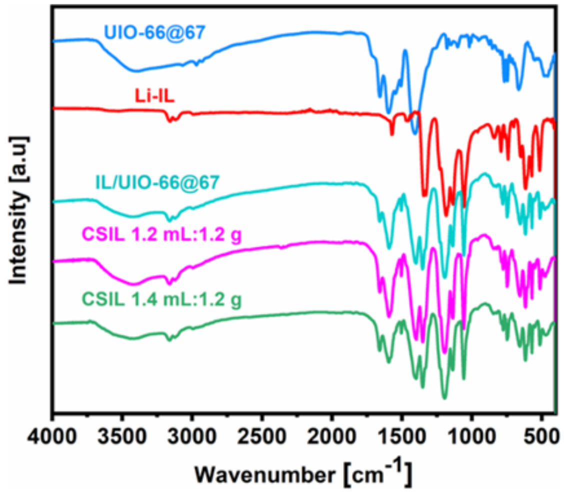

Figure S11. FT-IR spectra of CSLI with different Li-IL amount, core-shell with ionic liquid, pristine Li-IL and pristine MOF.

Regarding UIO-66@67/Li-IL electrolyte, all peaks indexed to UIO-66@67 and Li-IL. Comparing between MOF UIO/Li-IL and MOF UIO/IL (without Li^+ salt) spectra, we cannot find any additional peaks related to the bonds of lithium ions in UIO-66@67. Therefore, lithium ions are free in the CSIL solid electrolyte.

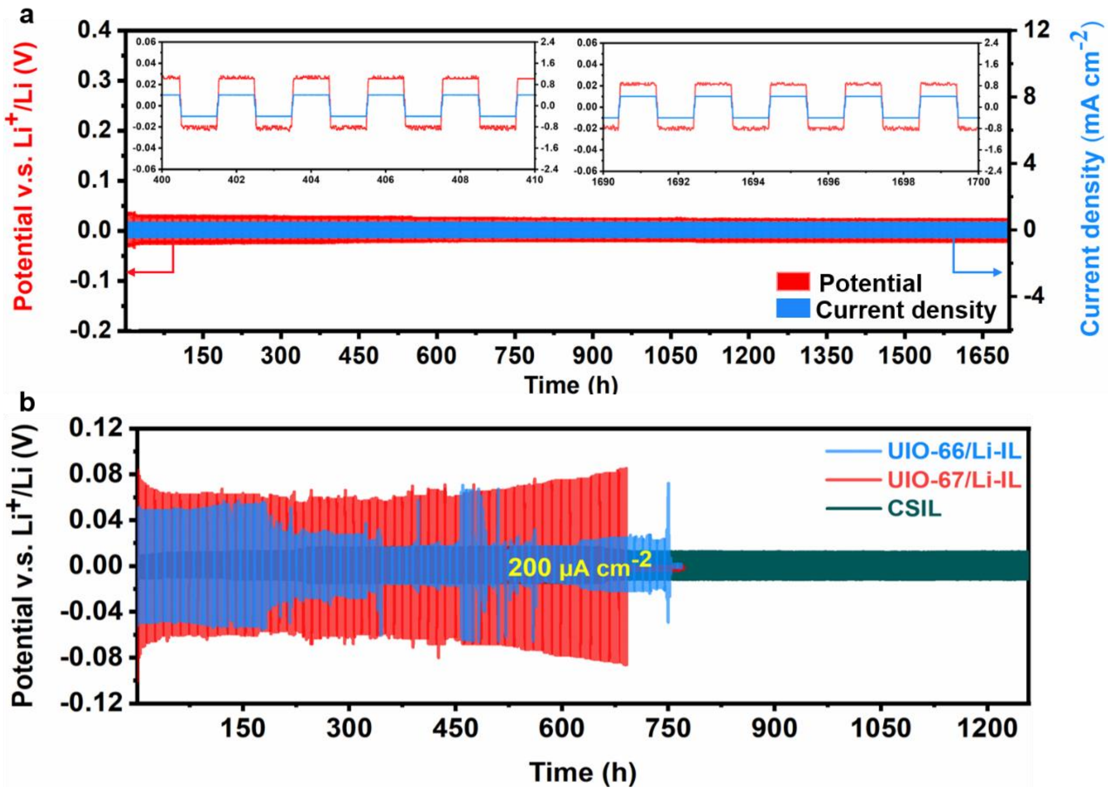

Figure S12. a) Voltage profile of the Li/CSIL/Li symmetric battery at a current density of 400 μA cm^{-2} Insets: detailed voltage profiles of the 400–410 h and 1400–1410 h, respectively. b) Comparison between voltage profiles of the Li/CSIL/Li, Li/UIO-66-Li-IL/Li, and Li/UIO-67-Li-IL/Li symmetric batteries at a current density of 200 μA cm^{-2}. All tests were performed at room temperature.

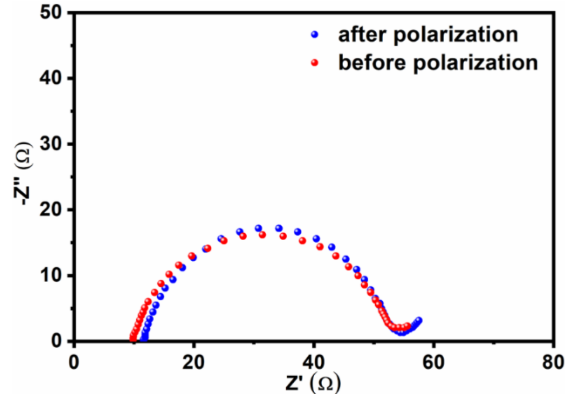

Figure S13. AC impedance spectra of CSIL before and after the galvanostatic cycling at 1000 µA cm^{-2} and room temperature.

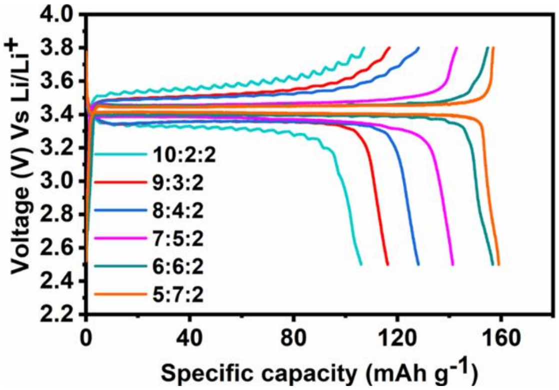

Figure S14. Typical charge/discharge profiles of LFP/CSIL/Li solid-state battery with different compositions of cathode LFP/CSIL/acetylene black (5:7:2, 6:6:2, 7:5:2, 8:4:2, 9:3:2 and 10:2:2) at 0.2C and 25 ˚C.

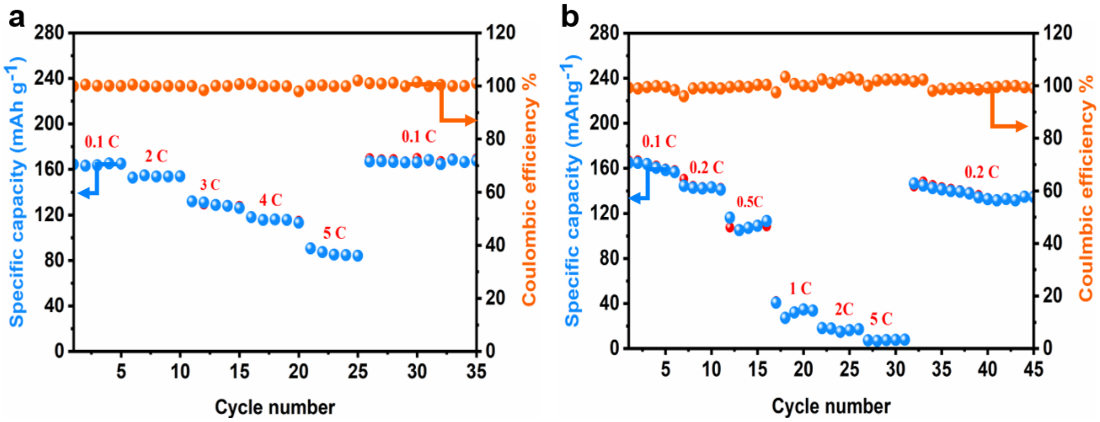

Figure S15. Cycling stability with Coulombic efficiency under different current rates (a) CSIL and (b) Li-IL with Li/$LiFePO_4$ cells at room temperature and 4 mg cm^{-2} cathode active material.

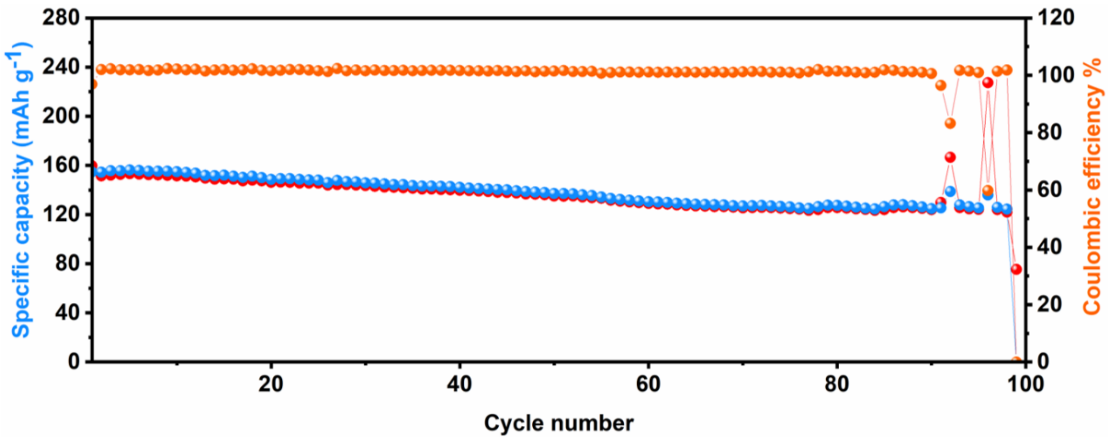

Figure S16. Cycling stability with Coulombic efficiency of Li/IL/LFP batteries under 0.2 C at room temperature.

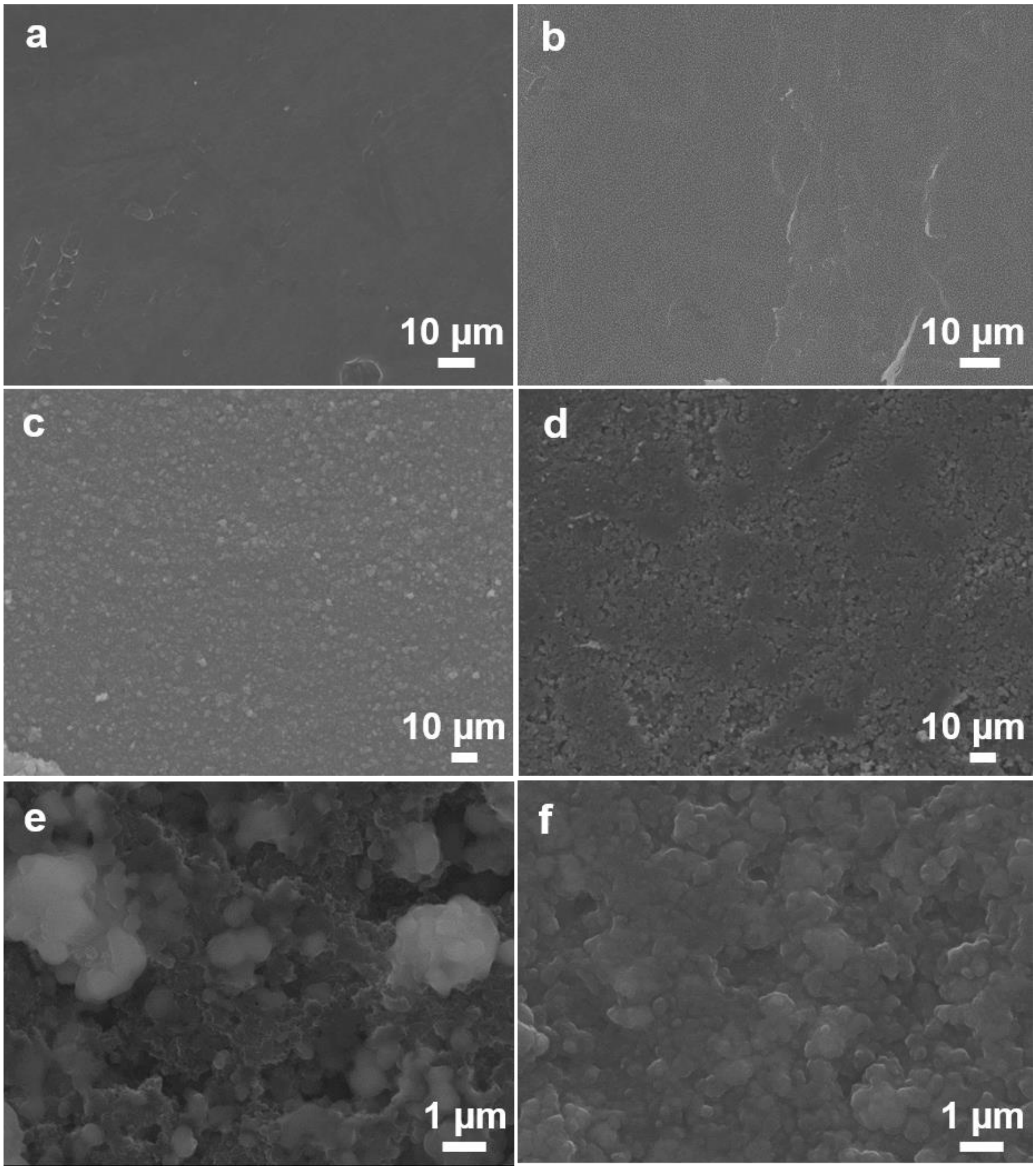

Figure S17. SEM images of (a, b) lithium electrode before and after cycling, (c, d) CSIL solid electrolyte before and after cycling, (e, f) LFP electrode before and after charge /discharge cycling 0.2 C and room temperature.

Table S1. Comparison for ionic conductivity and Li^+ transference number of CSIL solid electrolyte and other MOF-based electrolytes.

Type of electrolyte	**σ (S cm^{-1})**	t_{Li^+}	**Ref.**
LPC@UIO-67	6.5×10^{-4} (27 °C, 100 mV)	0.65 (27 °C, 20 mV)	[1]
UIO-66/Li-IL	3.2×10^{-4} (25 °C, 50 mV)	0.33 (27 °C, 10 mV)	[2]
UIO-67/Li-IL/LLZO	1×10^{-4} (30 °C)	0.18 (27 °C, 10 mV)	[3]
MOF-688/PC	3.4×10^{-4} (20 °C)	0.87 (27 °C)	[4]
MOF-525(Cu)- Li-IL	3×10^{-4} (27 °C)	0.36 (27 °C, 10 mV)	[5]
PEO- ZIF-8	4.7×10^{-4} (25 °C, 5 mV)	0.68 (25 °C, 10 mV)	[6]
Cu2(BPY)2(NDIDS)	2.3×10^{-4} (28 °C)	-----	[7]
ZIF-67/IL	2.29×10^{-3} (30 °C)	-----	[8]
IL	8.4×10^{-3} (25 °C)	0.3 (25 °C)	[9]
CSIL	2.4×10^{-3} (25 °C, 100 mV)	0.63 (25 °C, 10 mV)	Our work

Table S2. Comparison for electrochemical performance of CSIL solid electrolyte and other MOF-based electrolytes.

Type of electrolyte	**Lithium compatibility**	**Capacity mAhg^{-1}/ No. of cycles, retention**	**Cathode composition/loading amount**	**Ref.**
LPC@UIO-67	1200 cycles at 125 μA cm^{-2} and 27 ^{o}C	125/500, retention 75% at 1 C and 27 ^{o}C	LFP, acetylene black, PVdF (7:2:1) / 2 mg cm^{-2}.	1
UIO-66/Li-IL	100 cycles at 200 μA cm^{-2} and 60 ^{o}C	130 /100, retention 100% at 0.2 C and 60 ^{o}C	LFP, UIO-Li-IL, Ketjen black (4:4:2)/ 1–2 mg cm^{-2}	2
20%UIO67-Li-IL/ LLZO	900 cycles at 100 μA cm^{-2} and 27 ^{o}C	140/150, retention 97% at 0.1 C and 27 ^{o}C	LFP, UIO-Li-IL, acetylene black (5:4:1)/ 13 mg cm^{-2}	3
MOF-688/PC	-	130/200, retention 92% at 0.2 C and 27 ^{o}C	LFP, MOF, Super C45, PVdF (5:3:1:1)/ 2 mg cm^{-2}	4
MOF-525(Cu)-Li-IL	800 cycles at 200 μA cm^{-2} and 27 ^{o}C	145/100, retention 90% at 0.1 C and 27 ^{o}C	LFP, UIO-Li-IL, acetylene black (5:5:2)/ 25 mg·cm^{-2}	5
PEO- ZIF-8	800 cycles at 100 μA cm^{-2} and 25 ^{o}C	117/300, retention 89% at 1 C and 25 ^{o}C	LFP, super P, PVdF (8:1:1) / 4-5 mg cm^{-2}.	6
IL	30 cycles at 200 μA cm^{-2} and 25 ^{o}C	160/5, at 0.2 C and 25 ^{o}C 19.2/5, at 1 C and 25 ^{o}C	LFP, PVdF , C black (7.8:1:1.2) / 2.31 mg cm^{-2}.	9
CSIL	1050 cycles at 1000 μA cm^{-2} and 25 ^{o}C	158/100, retention 99% at 0.2 C and 25 ^{o}C	LFP, UIO-Li-IL, acetylene black (6:6:2)/ 2 mg cm^{-2}	Our work

References

[1] L. Shen, H. B. Wu, F. Liu, J. L. Brosmer, G. Shen, X. Wang, J. I. Zink, Q. Xiao, M. Cai, G. Wang, Y. Lu, B. Dunn, Adv. Mater. 2018, 30, 1707476.

[2] J.-F. Wu, X. Guo, Small 2019, 15, 1804413.

[3] Z. Wang, Z. Wang, L. Yang, H. Wang, Y. Song, L. Han, K. Yang, J. Hu, H. Chen, F. Pan, Nano Energy 2018, 49, 580.

[4] W. Xu, X. Pei, C. S. Diercks, H. Lyu, Z. Ji, O. M. Yaghi, J. Am. Chem. Soc. 2019, 141, 17522.

[5] Z. Wang, R. Tan, H. Wang, L. Yang, J. Hu, H. Chen, F. Pan, Adv. Mater. 2018, 30, 1704436.

[6] G. Wang, P. He, L.-Z. Fan, Adv. Funct. Mater. 2020, 31, 3, 2007198.

[7] D. K. Panda, K. Maity, A. Palukoshka, F. Ibrahim, S. Saha, ACS Sustainable Chem. Eng. 2019, 7, 4619.

[8] N. Chen, Y. Li, Y. Dai, W. Qu, Y. Xing, Y. Ye, Z. Wen, C. Guo, F. Wu, R. Chen, J. Mater. Chem. A 2019, 7, 9530.

[9] M. Safa, A. Chamaani, N. Chawla, B. El-Zahab, Electrochimica Acta 2016, 213, 587-593.